FANTASI: A Novel Devices-to-Circuits Simulation Framework for Fast Estimation of Write Error Rates in Spintronics

Venkata Pavan Kumar Miriyala
Dept. of Elect. & Comp. Engineering
National University of Singapore
Singapore, 119077.
elevpkm@nus.edu.sg

Xuanyao Fong
Dept. of Elect. & Comp. Engineering
National University of Singapore
Singapore, 119077.
kelvin.xy.fong@nus.edu.sg

Gengchiau Liang
Dept. of Elect. & Comp. Engineering
National University of Singapore
Singapore, 119077.
elelg@nus.edu.sg

***Abstract*—Though physical mechanisms such as spin-transfer torque (STT), spin-orbit torque (SOT), and voltage-controlled magnetic anisotropy (VCMA) has potential to enable energy-efficient and ultra-fast switching of spintronic devices, the switching dynamics are stochastic due to thermal fluctuations. Thus, there is a need in spintronics to understand the interactions between circuit design and the error rate in the switching mechanism, called as write error rate. In this paper, we propose a novel devices-to-circuits simulation framework (FANTASI) for fast estimation of the write error rates (WER) in different spintronic devices and circuits. Here, we show that, FANTASI enables efficient spintronic device-circuit co-design, with results in good agreement with the experimental measurements.**

***Index Terms*—Spin-transfer torque, spin-orbit torque, voltage-controlled magnetic anisotropy, Fokker-Planck equation, spintronics**

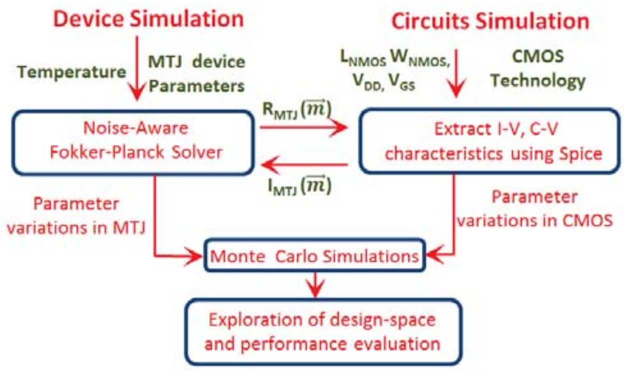

Fig. 1. Flow chart of the developed device-to-circuits level simulation framewok.

I. Introduction

In last two decades, spintronics has successfully emerged as a promising beyond-CMOS technology for realizing energy-efficient memory [1], logic [2] and diverse functional devices such as oscillators [3], random-number generators [4], artificial neurons [5], etc. However, the thermal noise acting on spintronic devices introduces randomness in their switching dynamics. Therefore, the switching process becomes probabilistic and the write error rate (WER) [6] needs to be accurately estimated to enable design of reliable spintronic devices and circuits.

Using the Monte Carlo (MC) approach with the simulation framework presented in [7] requires at least 15×10^6 hours to generate 10^9 simulation samples to capture WER of 10^{-9}. This poses a significant challenge to spintronic device-circuit co-design, especially when the impact of process variations on the interactions between spintronic devices and various circuit elements needs to be investigated. In the proposed simulation framework (FANTASI), the state of the spintronic device (i.e., magnetization) is modeled as a probability density function (PDF) and the Fokker-Planck equation (FPE) [8] is solved to capture the time evolution of the PDF. As compared to [8], the FPE in FANTASI has been modified to capture the interaction between various spintronic device physics, and the effect of circuit elements. FANTASI requires 15–30 minutes of run time to capture WER of 10^{-9}, which is 30×10^6 times faster than the conventional MC approach. In addition, FANTASI can be successfully calibrated against the experimental measurements of different spintronic devices.

For the rest of this paper, Section II describes the proposed devices-to-circuits simulation framework, which we call as FANTASI. Section III then discusses the simulation results obtained for different spintronic devices and their benchmarking against experimental measurements. Finally, Section IV concludes this paper. For convenience, the symbols used in the rest of this manuscript are listed in Table I.

II. Simulation Framework

The simulation methodology of FANTASI is illustrated in Fig. 1. To model the electrical interactions between circuit elements, such as the CMOS transistor, and the spintronic devices, conventional circuit simulation tools such as SPICE can be used to determine the electrical stimulus applied to the spintronic device. In FANTASI, SPICE simulation results are

The work is funded in part by the National University of Singapore Faculty Research Committee Start-up Grant, and by the Singapore Ministry of Education Academic Research Fund Tier 1.

used by the noise-aware Fokker-Planck (FP) solver to estimate the WER of the spintronic devices in a single simulation run. Thus, the number of MC simulation samples required to explore the design space of the spintronic circuit under thermal noise and process variations may be significantly reduced using FANTASI (see the flow chart depicted in Fig. 1).

A. Thermal Noise-Aware Fokker-Planck Solver

The FPE, given as

$$\frac{d\rho}{dt} = -\boldsymbol{\nabla}\left(\rho(\boldsymbol{m}) \cdot \boldsymbol{\vartheta}(\boldsymbol{m})\right) - D\boldsymbol{\nabla}^2\rho(\boldsymbol{m}) \tag{1}$$

captures the effect of thermal fluctuations by modeling the PDF of magnetization ($\boldsymbol{m}$) of the spintronic device. The PDF of $\boldsymbol{m}$, $\rho(\boldsymbol{m})$, allows us to calculate the probability of finding $\boldsymbol{m}$ in any region of its state space, which is the surface of a unit sphere. The time evolution of $\rho(\boldsymbol{m})$ is described using drift and diffusion terms; the drift term models the deterministic behavior due to several physical effects (i.e., STT, SOT, VCMA, etc.) and the diffusion term models the effect of thermal fluctuations.

The drift term (the first term on the right-hand side of (1)) uses the velocity, $\boldsymbol{\vartheta}(\boldsymbol{m})$, to model the effect of deterministic forces on $\boldsymbol{m}$. $\boldsymbol{\vartheta}(\boldsymbol{m})$ at every point in the state space of $\boldsymbol{m}$ is obtained using the Landau-Lifshitz-Gilbert-Slonczewski (LLGS) equation [9]–[10], written as

$$\begin{aligned}\left(1+\alpha^2\right)\frac{d\boldsymbol{m}}{dt} &= -\mu_0\gamma\boldsymbol{m}\times\left(\boldsymbol{H}_{\text{eff}}+\alpha\boldsymbol{m}\times\boldsymbol{H}_{\text{eff}}\right)\\ &\quad -\beta\boldsymbol{m}\times\left[\epsilon\left(\boldsymbol{m}\times\boldsymbol{m}_{\text{p}}\right)-\epsilon'\boldsymbol{m}_{\text{p}}\right]\end{aligned} \tag{2}$$

$$\boldsymbol{H}_{\text{eff}} = \boldsymbol{H}_{\text{anis}} + \boldsymbol{H}_{\text{demag}} + \boldsymbol{H}_{\text{ext}}, \boldsymbol{H}_{\text{anis}} = H_{\text{k}} \cdot m_{\text{z}} \cdot \hat{\boldsymbol{z}} \tag{3}$$

$$H_{\text{k}} = \frac{2K_{\text{eff}}}{\mu_0 M_{\text{S}}(T)}, K_{\text{eff}} = K_{\text{u}} + \frac{K_{\text{I}}(T)}{t_{\text{FL}}} - \left(\frac{\xi(T)V_{\text{MTJ}}}{t_{\text{OX}}t_{\text{FL}}}\right) \tag{4}$$

$$\boldsymbol{H}_{\text{demag}} = -N_{\text{xx}} \cdot m_{\text{x}} \cdot \hat{\boldsymbol{x}} - N_{\text{yy}} \cdot m_{\text{y}} \cdot \hat{\boldsymbol{y}} - N_{\text{zz}} \cdot m_{\text{z}} \cdot \hat{\boldsymbol{z}} \tag{5}$$

$$\beta = \frac{\hbar\gamma J_{\text{MTJ}}}{2\mu_0 e t_{\text{FL}} M_{\text{S}}}, \epsilon = \frac{P\cdot\Lambda}{(\Lambda^2+1)+(\Lambda^2-1)\left(\boldsymbol{m}\cdot\boldsymbol{m}_{\text{p}}\right)} \tag{6}$$

The LLGS equation (2) describes the magnetization dynamics induced by effective magnetic field ($\boldsymbol{H}_{\text{eff}}$), and current-induced torques like STT or SOT given by equations (3)–(6). $\boldsymbol{H}_{\text{eff}}$ consists of the anisotropic ($\boldsymbol{H}_{\text{anis}}$), the demagnetizing ($\boldsymbol{H}_{\text{demag}}$) and the externally applied field ($\boldsymbol{H}_{\text{ext}}$). H_{k} is the net anisotropic field. β, ϵ, and ϵ' are the prefactors for the current-induced torques.

On the other hand, the diffusion term of (1), captures the effect of thermal fluctuations by spreading out $\rho(\boldsymbol{m})$ uniformly over the state space. The temperature dependent diffusion constant, D, determines the rate at which $\rho(\boldsymbol{m})$ spreads out in the state space and can be defined as

$$D = \frac{\alpha\gamma k_{\text{B}}T}{\left(1+\alpha^2\right)\mu_0\nu M_{\text{S}}} \tag{7}$$

In FANTASI, we numerically solve the (1). To estimate the WER of the spintronic device, the state space of $\boldsymbol{m}$ (the surface of the unit sphere) is partitioned into top (positive m_{z}) and bottom hemispheres (negative m_{z}). When considering magnetization switching from positive m_{z} to negative m_{z}, the probability of $\boldsymbol{m}$ remaining in the top hemisphere after write operation is performed is considered as the WER of the device.

TABLE I
LIST OF SYMBOLS

Symbol	Quantity
μ_0	Vacuum permeability
γ	Gyromagnetic ratio
α	Damping constant
$\hbar$	Reduced Plancks constant
k_{B}	Boltzmann constant
e	Electron charge
M_{S}	Saturation magnetization
ν	Volume of the ferromagnet
N_{xx}, N_{yy}, N_{zz}	Demagnetizing tensor values
K_{u}	Bulk anisotropy
K_{I}	Interfacial anisotropy
K_{eff}	Effective anisotropy
t_{FL} and t_{OX}	Thickness of free layer and oxide layer
E_{b}	Energy barrier
P	Polarization of ferromagnet
Λ	fitting parameter
V_{bias}	Bias voltage at which TMR is divided by 2
T^*	fitting parameter

*In this work, P = 0.56, Λ = 1.2, V_{bias} = 0.45 V, T^* = 1120 K.

B. Modeling of the Magnetic Tunelling Junction

The magnetic tunneling junction (MTJ) [11] is a fundamental component in most of the practical spintronic devices and circuits. MTJs consist of an oxide layer sandwiched between two ferromagnetic (FM) layers. One of the FM layers is magnetically pinned (pinned layer, PL) whereas the magnetization of other FM layer (free layer, FL) can be switched to be parallel (P) or anti-parallel (AP) with the magnetization of the PL. Due to the tunneling magnetoresistance (TMR) effect, the resistance across the MTJ, R_{MTJ}, is low and high when the MTJ is in P and AP configurations, respectively. In FANTASI, R_{MTJ} is modeled as [12]

$$R_{\text{MTJ}} = R_{\text{P}} + \frac{R_{\text{AP}}-R_{\text{P}}}{1+\left(\frac{V_{\text{MTJ}}}{V_{\text{bias}}}\right)^2}\left(\frac{1-\boldsymbol{m}\cdot\boldsymbol{m}_{\text{p}}}{2}\right) \tag{8}$$

In addition, the electrons flowing between PL and FL induce spin-transfer torque (STT) on the FL magnetization. If the torque is sufficiently large, the MTJ can be switched to either P or AP configuration. This switching mechanism can be modelled by considering J_{MTJ} in (6) as the current density flowing through the MTJ. In (6), $P \in [0,1]$ and $\Lambda \in [1,+\infty)$.

Furthermore, it is experimentally observed that, voltage applied across the MTJ, V_{MTJ} significantly reduces H_{k} and results in ultra-fast and energy-efficient switching of the MTJ [13]. In FANTASI, VCMA switching can be modeled using a voltage-dependent variable in the H_{k}, as shown in (4).

C. Modeling of Three-Terminal Spintronic Devices

MTJs can also be switched as in the case of three-terminal devices based on the spin Hall effect [14]. Depending on the spin Hall angle (θ_{SH}), the charge current flowing through the heavy metal (HM) generates a pure spin current that can switch the magnetization of the MTJ. The torques generated by such spin currents can be modelled by considering J_{MTJ} in (6) as $\theta_{\mathrm{SH}} \cdot J_{\mathrm{HM}}$. P and Λ in (6) are considered to be 1, and J_{HM} is the current density flowing through the HM.

Note also that the temperature dependence of different material parameters such as $M_{\mathrm{S}}(T)$, $K_{\mathrm{I}}(T)$, and $\xi(T)$ are captured in FANTASI by modeling them as [15]

$$M_{\mathrm{S}}(T) = M_{\mathrm{S}}(0)(1 - (T/T^{*})^{1.5}) \tag{9}$$

$$K_{\mathrm{I}}(T) = K_{\mathrm{I}}(0)(M_{\mathrm{S}}(T)/M_{\mathrm{S}}(0))^{2.18} \tag{10}$$

$$\xi(T) = \xi(0)(M_{\mathrm{S}}(T)/M_{\mathrm{S}}(0))^{2.83} \tag{11}$$

III. Simulation Results

In this section, we calibrate FANTASI against the experimental measurements of different spintronic devices. The voltage-dependence of WERs in STT MRAM are calculated by neglecting the VCMA effect. The voltage and size dependence of the WER in STT MRAM was experimentally characterized in [6]. As shown in Fig. 2 (a), our simulation results are in good agreement with the experimentally measured WERs for an MTJ with 40 nm diameter. Simulation parameters used for this calibration are listed in Table II, and compared with the experimentally extracted values. Next, we validate FANTASI for VCMA-based MTJs by reproducing the experimental data reported in [13]. We calculated the pulse duration dependent switching probabilities of VCMA-based MTJ till 0.8 ns, which is the region of interest for fast write operations. The simulation results match closely with the experimental data as shown in Fig. 2 (b). The parameters used for this calibration are listed in Table III, and compared with the experimentally extracted values.

Furthermore, our simulation framework is also useful in studying SOT-based spin torque nano-oscillators (SSTNO). We simulated the operation of an SSTNO with the structure shown in Fig. 3 (a). Results (see Fig. 3 (b)) from a single simulation in FANTASI show that under the applied stimulus, the SSTNO oscillates steadily in the presence of thermal agitations. The effort needed to reproduce similar results using the MC approach is expected to be significantly greater than FANTASI because it depends on oscillation frequency and the desired error margin.

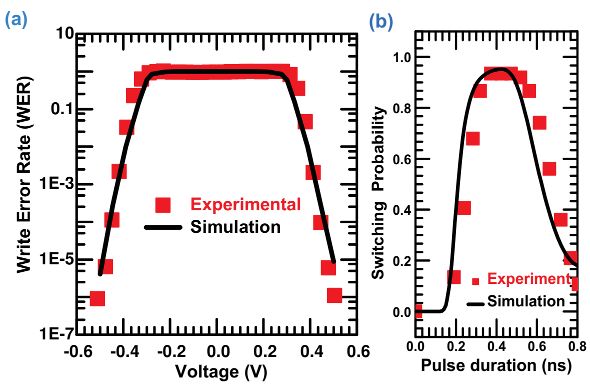

Fig. 2. Benchmarking of simulation results against experimental measurements of (a) STT, and (b) VCMA-based devices.

TABLE II
Parameters used for benchmarking of STT device

Symbol	Exp. Value	Sim. Value
M_{S}	$450 \times 10^3 A/m$	$450 \times 10^3 A/m$
α	-	0.0135
E_{b}	$44k_{\mathrm{B}}T$	$44k_{\mathrm{B}}T$
Diameter	40 nm	40 nm
Thickness	-	1 nm
TMR	53 %	53 %
Parallel-Resistance	6.4 KΩ	6.4 KΩ

TABLE III
Parameters used for benchmarking of VCMA device

Symbol	Exp. Value	Sim. Value
M_{S}	$625 \times 10^3 A/m$	$625 \times 10^3 A/m$
α	-	0.01
E_{b}	$30k_{\mathrm{B}}T$	$30k_{\mathrm{B}}T$
Diameter	50 nm	50 nm
Thickness	1.1 nm	1.1 nm
TMR	43 %	43 %
V_{MTJ}	2.1 V	2.1 V
H_{ext}	60 mT	60 mT
ξ	32 fJ/V·m	32 fJ/V·m
Resistance-Area (RA) Product	$650\ \Omega\text{-}\mu \cdot m^2$	$650\ \Omega\text{-}\mu \cdot m^2$

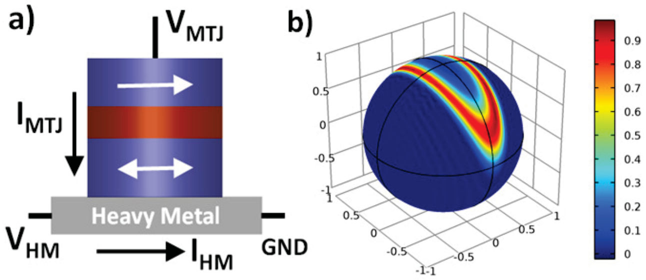

Fig. 3. (a) The schematic of SOT oscillator, and (b) the possible stable oscillation paths of $\boldsymbol{m}$ in the presence of thermal agitations at $300K$.

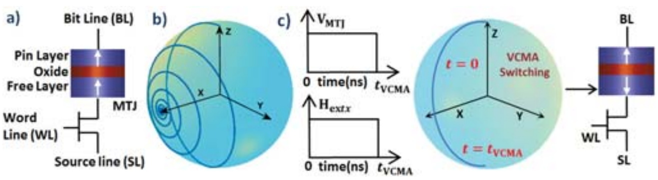

Fig. 4. (a) The schematic of VCMA MRAM bit-cell consisting of a p-MTJ and an NMOS access transistor. (b) Due to VCMA effect, the voltage drop (V_{MTJ}) across the MTJ changes the perpendicular easy-axis of the free layer (FL) to the in-plane direction, leading to continuous precession of FLs magnetization ($\boldsymbol{m}$) around the new in-plane easy axis $\boldsymbol{x}$. (c) By precisely timing V_{MTJ} and external field (H_{extx}) to half-precession period (t_{VCMA}), $\boldsymbol{m}$ can be switched from positive $\boldsymbol{z}$ (parallel configuration) to negative $\boldsymbol{z}$ (anti-parallel configuration).

TABLE IV
PARAMETERS USED FOR VCMA-MRAM ANALYSIS

Symbol	Value at 300K
M_S	$1257 \times 10^3 A/m$
α	0.01
Dimensions of FL	150 nm, 50 nm, 1.7 nm
t_{OX}	2 nm
TMR	144 %
K_u	$2.245 \times 10^5 J/m^3$
K_I	$1.286 \times 10^{-3} J/m^2$
ξ	50 fJ/V·m
RA Product	1820 Ω-$\mu \cdot m^2$

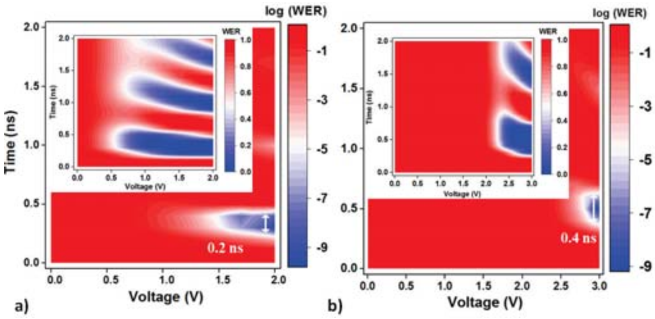

Fig. 5. The dependence of WERs on write voltage and pulse duration in VCMA MRAMs using (a) 50 mT, and (b) 30 mT of external field at 300K. Parameters used in obtaining these results are tabulated in Table IV.

A detailed analysis of VCMA MRAM bit-cells may also be performed using FANTASI. A voltage pulse and an external magnetic field are used to switch the MTJ in the bit-cell shown in Fig. 4. Fig. 5 shows the dependence of WERs on write voltage, time pulse duration, and external magnetic fields. In Fig. 5 (a), WER of 10^{-9} is acheived when the pulse width is in the range of 0.2–0.4 ns, which implies the need for precise control of the voltage pulse duration. Reducing the external field from 50 mT to 30 mT increases the pulse width range to 0.3–0.7 ns as shown in Fig. 5 (b), but at the cost of higher write voltages. Using higher input voltages increases the energy consumed in charging and discharging of the memory control lines [16]. The results also highlight the possibility of attaining ultra-fast (0.3 ns) switching at WER of 10^{-9} with 2 fJ of switching energy (considering only ohmic losses across the MTJ and the charging of the MTJ capacitance). FANTASI also enables analysis of the impact of process, voltage and temperature (PVT) variations on the VCMA based MTJ. Fig. 6 (a)–(b) show that increasing the temperature from 300 K to 350 K significantly increases the WER (from 10^{-9} to 10^{-5}) and no switching is observed at 400 K. Fig. 6 (c)–(d) show that variations in the energy barrier of the MTJs significantly reduce the design space. Increase in the energy barrier from 139 k_BT to 174 k_BT increases the WER from 10^{-9} to 10^{-2}. However, the operation window for the voltage pulse duration has been increased from 0.25 ns to 0.4 ns. The impact of process variations in the NMOS access transistor on the WER of VCMA MRAM is studied using FANTASI by considering a Gaussian distribution for

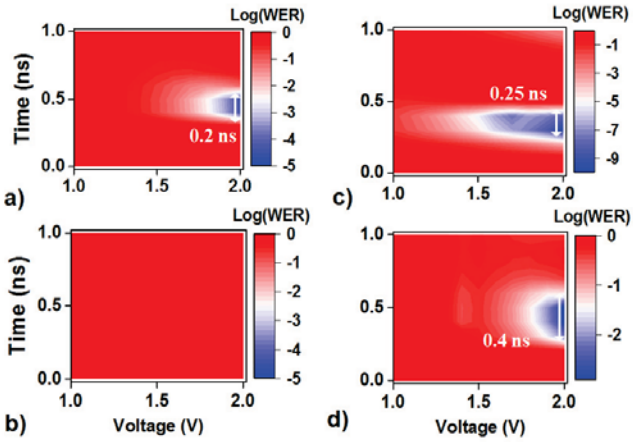

Fig. 6. The dependence of WERs at (a) 350K and (b) 400K and, energy barriers of (c) 139 k_BT and (d) 174 k_BT.

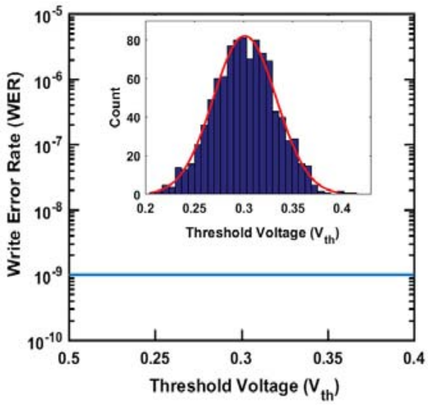

Fig. 7. The dependence of WERs on process (V_{th}) variations of CMOS (45 nm transistor). The inset shows the distribution of V_{th} due to process variations. The blue line shows the WER of the VCMA MRAM, which is maintained constant at 10^{-9}. The change in the WER due to fluctuations in V_{th} is found to be negligible ($< 10^{-10}$).

the threshold voltage of the access transistor. Fig. 7 shows that process variations in the NMOS access transistor have negligible effect on the WER of VCMA MRAM since most of the voltage applied between BL and SL is dropped across the VCMA based MTJ.

IV. CONCLUSION

In summary, we proposed a novel devices-to-circuits simulation framework (FANTASI) for fast estimation of write error rates in spintronic devices and circuits, and showed that it can be successfully calibrated to the experimental data of STT MRAM and VCMA based MTJs. An SOT-based spin torque nano-oscillator (SSTNO) is modeled to illustrate the efficiency of FANTASI in studying the behavior of SSTNOs in the presence of thermal agitations. Finally, the influence of process, voltage and temperature variations on WERs of VCMA based memory devices is studied. The intrinsic energy consumed during the VCMA switching is found to be as low as 2 fJ with WER of 10^{-9} and write delay of 0.3 ns.

REFERENCES

[1] T. Endoh, H. Koike, S. Ikeda, T. Hanyu, and H. Ohno, "An overview of non-volatile emerging memories-spintronics for working memories," IEEE J. Emerg. Sel. Topic Circuits Syst., vol. 6, no. 2, pp. 109-119, Jun. 2016.

[2] S. Manipatruni, D. E. Nikonov, I. A. Young, "Beyond CMOS computing with spin and polarization," Nat. Phys., vol. 14, pp. 338–343, Apr. 2018.

[3] A. Slavin, and V. Tiberkevich, "Nonlinear Auto-Oscillator Theory of Microwave Generation by Spin-Polarized Current," in IEEE Trans. Magn., vol. 45, no. 4, pp. 1875–1918, Apr. 2009.

[4] A. Fukushima, T. Seki, K. Yakushiji, H. Kubota, H. Imamura, S. Yuasa, and K. Ando, "Spin dice: A scalable truly random number generator based on spintronics," Appl. Phys. Exp., vol. 7, no. 8, p. 083001, Jul. 2014.

[5] X. Fong, Y. Kim, K. Yogendra, D. Fan, A. Sengupta, A. Raghunathan, and K. Roy, "Spin-Transfer Torque Devices for Logic and Memory: Prospects and Perspectives," IEEE Trans. Comput.-Aided Design Integr. Circuits Syst., vol. 35, no. 1, pp. 1-22, Jan. 2016.

[6] J. J. Nowak, R. P. Robertazzi, J. Z. Sun, G. Hu, J. Park, J. Lee, A. J. Annunziata, G. P. Lauer, R. Kothandaraman, E. J. OSullivan, P. L. Trouilloud, Y. Kim, and D. C. Worledge, "Dependence of voltage and size on write error rates in spin-transfer torque magnetic random access memory," IEEE Magn. Lett., vol. 7, pp. 1-4, Jun. 2016.

[7] X. Fong, S. K. Gupta, N. N. Mojumder, S. H. Choday, C. Augustine and K. Roy, "KNACK: A hybrid spin-charge mixed-mode simulator for evaluating different genres of spin-transfer torque MRAM bit-cells," in Proc. Int. Conf. SISPAD, pp. 51-54, Sept. 2011.

[8] Y. Xie, B. Behin-Aein, and A. W. Ghosh, "Fokker-planck study of parameter dependence on write error slope in spin-torque switching," IEEE Trans. Electron Devices., vol. 64, no. 1, pp. 319-324, Jan. 2017.

[9] L. Landau and E. Lifshitz, "On the theory of the dispersion of magnetic permeability in ferromagnetic bodies," Phys. Z. Sowjet., vol. 8, pp. 153-169, Jan. 1935.

[10] T. L. Gilbert, "A phenomenological theory of damping in ferromagnetic materials," IEEE Trans. Magn., vol. 40, no. 6, pp. 3443-3449, Nov. 2004.

[11] S. Ikeda, K. Miura, H. Yamamoto, K. Mizunuma, H. D. Gan, M. Endo, S. Kanai, J. Hayakawa, F. Matsukura, and H. Ohno, "A perpendicular anisotropy CoFeB-MgO magnetic tunnel junction," Nat. Mater., vol. 9, pp. 721–724, Jul. 2010.

[12] W. F. Brinkman, R. C. Dynes, and J. M. Rowell, "Tunneling conductance of asymmetrical barriers," J. Appl. Phys., vol. 41, no. 5, pp. 1915-1921, Apr. 1970.

[13] C. Grezes, F. Ebrahimi, J. G. Alzate, X. Cai, J. A. Katine, J. Langer, B. Ocker, P. K. Amiri, and K. L. Wang, "Ultra-low switching energy and scaling in electric-field-controlled nanoscale magnetic tunnel junctions with high resistance-area product," Appl. Phys. Lett., vol. 108, p. 012403, Jan. 2016.

[14] L. Liu, C. Pai, Y. Li, H. W. Tseng, D. C. Ralph, R. A. Buhrman, "Spin-Torque Switching with the Giant Spin Hall Effect of Tantalum," Science, vol. 336, no. 6081, pp. 555–558, May. 2012.

[15] J. G. Alzate, P. K. Amiri, G. Yu, P. Upadhyaya, J. A. Katine, J. Langer, B. Ocker, I. N. Krivorotov, and K. L. Wang, "Temperature dependence of the voltage-controlled perpendicular anisotropy in nanoscale MgO—CoFeB—Ta magnetic tunnel junctions," Appl. Phys. Lett., vol. 104, no. 11, p. 112410, Mar. 2014.

[16] L. Xiaoyao, K. Turgay, and D. Brooks, "Architectural power models for SRAM and CAM structures based on hybrid analytical/empirical techniques," in Proc. ICCAD, no. 1, pp. 824-830, Nov. 2007.